Snap Transitions of Pressurized Graphene Blisters

Peng Wang
Department of Aerospace Engineering and Engineering Mechanics,
University of Texas,
Austin, TX 78712

Kenneth M. Liechti
Department of Aerospace Engineering and Engineering Mechanics,
University of Texas,
Austin, TX 78712

Rui Huang
Department of Aerospace Engineering and Engineering Mechanics,
University of Texas,
Austin, TX 78712

Blister tests are commonly used to determine the mechanical and interfacial properties of thin film materials with recent applications for graphene. This paper presents a numerical study on snap transitions of pressurized graphene blisters. A continuum model is adopted combining a nonlinear plate theory for monolayer graphene with a nonlinear traction–separation relation for van der Waals interactions. Three types of blister configurations are considered. For graphene bubble blisters, snap-through and snap-back transitions between pancake-like and dome-like shapes are predicted under pressure-controlled conditions. For center-island graphene blisters, snap transitions between donut-like and dome-like shapes are predicted under both pressure and volume control. Finally, for the center-hole graphene blisters, growth is stable under volume or N-control but unstable under pressure control. With a finite hole depth, the growth may start with a snap transition under N-control if the hole is relatively deep. The numerical results provide a systematic understanding on the mechanics of graphene blisters, consistent with previously reported experiments. Of particular interest is the relationship between the van der Waals interactions and measurable quantities in corresponding blister tests, with which both the adhesion energy of graphene and the equilibrium separation for the van der Waals interactions may be determined. In comparison with approximate solutions based on membrane analyses, the numerical method offers more accurate solutions that may be used in conjunction with experiments for quantitative characterization of the interfacial properties of graphene and other two-dimensional (2D) membrane materials.
[DOI: 10.1115/1.4033305]

Keywords: blister test, snap transition, graphene, adhesion

1 Introduction

Pressurized blister tests are commonly used to measure mechanical and adhesion properties of thin films and coatings [1–4]. Several types of blister tests have been developed, including the standard blister test, island blister test, constrained blister test, and peninsula blister test. Recently, similar blister tests have been applied to measure interfacial properties of graphene [5–8]. Using a center-island blister configuration, Liu et al. [9] observed pull-in instability of graphene membranes at ~10 nm separation. Although such a separation is considerably larger than typical ranges of van der Waals forces, it was found to be consistent with a theoretical model assuming long-range van der Waals interactions. In a subsequent study, Boddeti et al. [10] reported switchable shapes of graphene blisters using the same blister configuration. In this paper, we show by a numerical analysis that both the pull-in instability and the switchable blister shapes are results of snap transitions, a structural instability modulated by adhesive interactions. Moreover, it is suggested that such a blister test may be used to determine the two key parameters of van der Waals interactions between graphene and its substrate, including the adhesion energy and the equilibrium separation (as a length scale). The latter is typically less than 1 nm and thus difficult to determine by other experimental methods.

Besides specifically designed graphene blister tests, graphene bubble blisters are often observed when graphene membranes are placed on top of solid substrates [11,12]. Such graphene bubble blisters may form during transfer or growth processes with trapped gas or hydrocarbon residuals between the graphene membranes and the substrates since graphene is impermeable to most gases [13]. Irradiation of energetic protons or exposure to hydrofluoric acid (HF) and water (H_2O) vapors for etching could also cause formation of graphene bubble blisters due to accumulation of the chemically released gas from the substrate [11,14]. The observed graphene bubble blisters have diameters ranging from tens of nanometers to tens of microns, with a variety of shapes (circular, triangular, and diamond). Use of graphene nanobubbles has been suggested as a viable method for strain engineering to manipulate the electronic properties of graphene [15–18]. Microscale graphene bubble blisters have been used to study the Raman spectrum of graphene under biaxial strain [19]. In a previous study [20], analytical methods were developed to deduce the interfacial adhesion energy from measurements of the bubble blister size (height and radius). Subsequently, a more accurate solution was obtained by a numerical method, in comparison with the analytical solutions and molecular dynamics simulations [21]. The effect of van der Waals interactions was considered and a snap-back behavior was predicted for the graphene bubble blisters when the pressure difference drops to a critical level, similar to the pull-in instability observed for the center-island blisters [9]. In the present study, we consider both the graphene bubble blisters and the center-island blisters, with a focus on the snap transitions. Such snap transitions depend on the nonlinear interactions between graphene and its substrate, which may be exploited to experimentally characterize the adhesive properties of graphene and other thin membrane materials.

The remainder of this paper is organized as follows. Section 2 presents a continuum model combining a nonlinear plate theory for monolayer graphene and an analytical model for van der Waals interactions. Section 3 describes a numerical method to solve the nonlinear problem with snap transitions. Three types of blister configurations are then considered (Fig. 1): graphene bubble blisters in Sec. 4, center-island blisters in Sec. 5, and center-hole blisters in Sec. 6. The results are summarized in Sec. 7.

2 A Continuum Model for Graphene Blisters

In this paper, we consider three types of axisymmetric graphene blisters as illustrated in Fig. 1. The circular bubble blister has a radius a and height h (Fig. 1(a)). As the pressure inside the bubble

Contributed by the Applied Mechanics Division of ASME for publication in the Journal of Applied Mechanics. Manuscript received February 28, 2016; final manuscript received April 3, 2016; published online April 20, 2016. Editor: Yonggang Huang.

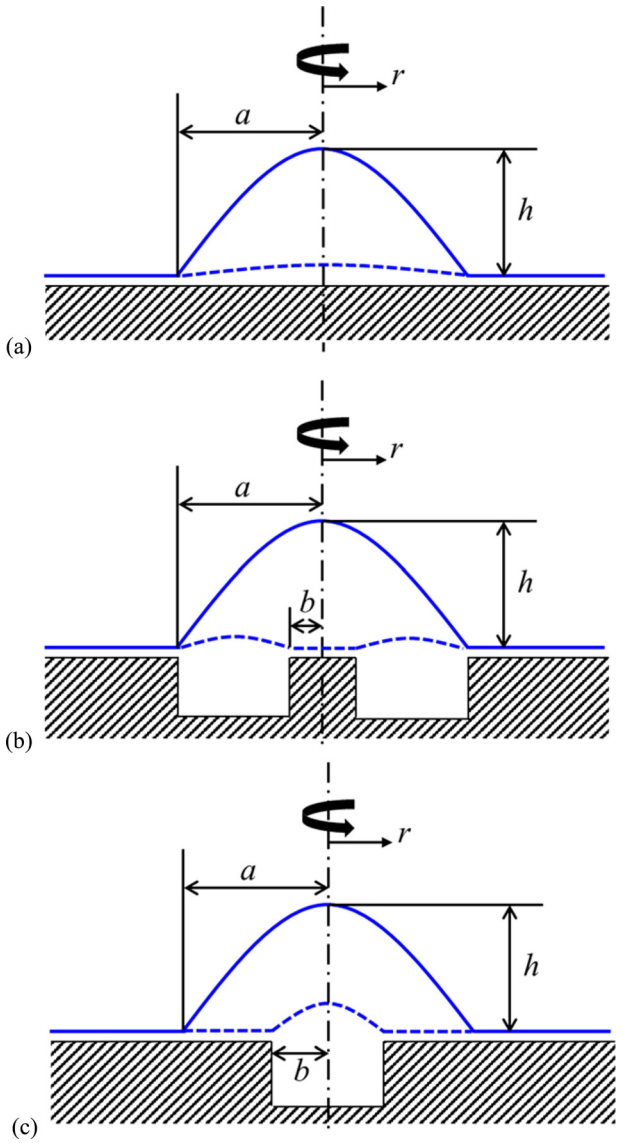

Fig. 1 Three types of graphene blisters: (*a*) a circular bubble blister with radius *a* and height *h*; (*b*) a center-island blister; and (*c*) a center-hole blister

changes, the height changes and may snap back to a nearly flat state due to the adhesive interaction with the substrate. The radius is assumed to be fixed, and the graphene outside the blister ($r > a$) is assumed to bond perfectly with the substrate. For the center-island blister (Fig. 1(*b*)), the substrate underneath the blister has been removed in the annular region ($b < r < a$), leaving behind a circular island at the center. As a result, the adhesive interaction is limited to the center region of the membrane ($r < b$). In this case, the snap transitions could occur between a dome-shaped blister and a donut-shaped with a flat center region. Finally, for the center-hole blister (Fig. 1(*c*)), the substrate has been removed in the center region ($r < b$) so that the adhesive interaction is limited to the annular region ($a > r > b$). This is the standard blister test configuration, which can have either stable or unstable growth of the blister radius by delamination. In all cases, we model the graphene as a continuum membrane and employ an analytical formula for the adhesive interaction, whereas the substrate is assumed to be rigid.

The mechanical behavior of a graphene monolayer can be described by a mixed continuum mechanics formulation mapping a 2D plane to a surface in the three-dimensional space [22,23]. The general kinematics of deformation is described by an in-plane Green-Lagrange strain tensor and a curvature tensor, both defined with respect to a reference state in 2D (i.e., the ground state of graphene). Under the assumption of small strain and moderately large deflection, the general formulation is reduced to a form similar to the nonlinear von Karman plate theory. In the present study, the axisymmetric formulation is used for circular graphene membranes subjected to axisymmetric loading, with two governing equations [21]:

$$\frac{d^2u}{dr^2}+\frac{1}{r}\frac{du}{dr}-\frac{u}{r^2}=-\frac{1-\nu}{2r}\left(\frac{dw}{dr}\right)^2-\frac{dw}{dr}\frac{d^2w}{dr^2} \tag{1}$$

$$D\left(\frac{d^3w}{dr^3}+\frac{1}{r}\frac{d^2w}{dr^2}-\frac{1}{r^2}\frac{dw}{dr}\right)-\frac{E_{2D}}{1-\nu^2}\frac{dw}{dr}\left(\frac{du}{dr}+\nu\frac{u}{r}+\frac{1}{2}\left(\frac{dw}{dr}\right)^2\right)=\frac{1}{r}\int_0^r qrdr \tag{2}$$

where $u_r = u(r)$ is the in-plane radial displacement and $w = w(r)$ is the out-of-plane deflection of graphene. The basic elastic properties of monolayer graphene include the 2D Young's modulus E_{2D}, Poisson's ratio ν, and the bending modulus D. Unlike classical plate theory, the bending modulus of monolayer graphene is not directly related to the in-plane Young's modulus and Poisson's ratio. Instead, it is determined from atomistic modeling as an independent property [24–26]. Here, we use the material properties obtained from first-principle density functional theory (DFT) calculations [24]: $E_{2D} = 349\,\text{N/m}$, $\nu = 0.149$, and $D = 1.5\,\text{eV}$.

Previous studies have noted that the graphene membrane is often subject to a pretension [6–9], and the blister behavior depends sensitively on the pretension. The effect of pretension (T_0) can be taken into account by including an additional term, $-T_0(dw/dr)$, on the left-hand side of Eq. (2). In the present study, we assume zero pretension ($T_0 = 0$).

On the right-hand side of Eq. (2), q is the lateral load intensity, which consists of a constant pressure p (or pressure difference if the outer pressure is considered) and a normal traction due to van der Waals interactions between graphene and the substrate, i.e., $q(r) = p - \sigma_{\text{vdW}}(r)$. By a simple analytical model of van der Waals interactions [27,28], the normal traction can be written as a function of the deflection

$$\sigma_{\text{vdW}}(w)=\frac{9\Gamma}{2\delta_0}\left[\left(\frac{\delta_0}{w+\delta_0}\right)^4-\left(\frac{\delta_0}{w+\delta_0}\right)^{10}\right] \tag{3}$$

where δ_0 is the equilibrium separation and Γ is the adhesion energy. The nonlinear traction–separation relation is shown in Fig. 2, where the separation is normalized by δ_0 and the traction is normalized by the maximum traction (strength), $\sigma_{\text{vdW}}^{\max} = 1.466\Gamma/\delta_0$. Measurements of the adhesion energy Γ have reported values from 0.09 to 0.45 J/m^2 for monolayer graphene on silicon oxide [5–7,29], although much larger values (up to 6 J/m^2) were reported for other substrate materials [30,31]. For the equilibrium separation δ_0, direct measurements are difficult and typical values from 0.3 to 0.9 nm were estimated from indirect measurements [32–34]. In the present study, we take $\delta_0 = 0.6$ nm and $\Gamma = 0.1$ J/m^2 unless specified otherwise.

3 Numerical Method

In this section, we present a numerical method to solve the coupled nonlinear equations, (1) and (2), using Riks method. For convenience, we define an effective length scale, $h_e = \sqrt{12(1-\nu^2)D/E_{2D}}$, and normalize the equations accordingly. In addition, we replace the deflection w with the angle of rotation, $\theta = dw/dr$, and discretize the two equations by a finite difference method, as presented in a previous paper [21]. As a

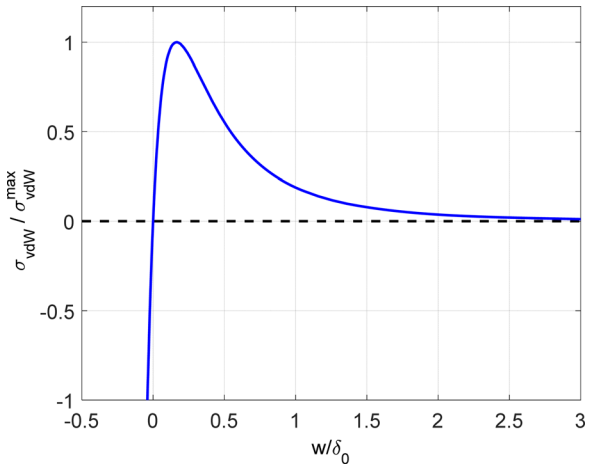

Fig. 2 Normalized traction–separation relation for van der Waals interactions between graphene and its substrate

result, we obtain a set of algebraic equations, $f_k(\boldsymbol{\theta}, \overline{\mathbf{u}}) = 0$ and $g_k(\boldsymbol{\theta}, \overline{\mathbf{u}}) = 0$, where

$$f_k = \frac{n^2}{\overline{a}^2}\left(1+\frac{1}{2k}\right)\theta_{k+1} - \frac{n^2}{\overline{a}^2}\left(2+\frac{1}{k^2}\right)\theta_k + \frac{n^2}{\overline{a}^2}\left(1-\frac{1}{2k}\right)\theta_{k-1} - \frac{6n}{\overline{a}}\theta_k(\overline{u}_{k+1}-\overline{u}_{k-1}) - \frac{12\nu n}{k\overline{a}}\theta_k\overline{u}_k - 6\theta_k^3 - \xi_k \tag{4}$$

$$g_k = \frac{n^2}{\overline{a}^2}\left(1+\frac{1}{2k}\right)\overline{u}_{k+1} - \frac{n^2}{\overline{a}^2}\left(2+\frac{1}{k^2}\right)\overline{u}_k + \frac{n^2}{\overline{a}^2}\left(1-\frac{1}{2k}\right)\overline{u}_{k-1} + \frac{(1-\nu)n}{2k\overline{a}}\theta_k^2 + \frac{n}{2\overline{a}}\theta_k(\theta_{k+1}-\theta_{k-1}) \tag{5}$$

for each internal node $(0<r<a)$ with $k=1$ to $n-1$ and $\xi_k = \overline{a}/(2nk)\left(\sum_{m=1}^{k-1} 2m\overline{q}_m + k\overline{q}_k\right)$. The boundary conditions are specified for the end nodes with $k=0$ and n: $\theta_0 = \theta_n = 0$ and $\overline{u}_0 = \overline{u}_n = 0$. Moreover, with $\overline{w}_n = 0$ at the edge of the blister $(r=a)$, we calculate the deflection at each node by numerically integrating the angle of rotation:

$$\overline{w}_k = -\frac{\overline{a}}{2n}\sum_{m=k}^{n-1}(\theta_m + \theta_{m+1}) \tag{6}$$

for $k=0$ to $n-1$, and the center deflection is then obtained as $h = w_0$.

The effect of the van der Waals force is included in the last term of Eq. (4), with

$$\overline{q}_k = \overline{p} - \overline{\sigma}_{\mathrm{vdW}}(\overline{w}_k) \tag{7}$$

and

$$\overline{\sigma}_{\mathrm{vdW}}(\overline{w}) = \overline{\Gamma}\left[\left(\frac{\overline{\delta}_0}{\overline{w}+\overline{\delta}_0}\right)^4 - \left(\frac{\overline{\delta}_0}{\overline{w}+\overline{\delta}_0}\right)^{10}\right] \tag{8}$$

where $\overline{p} = ph_e^3/D$, $\overline{\sigma}_{\mathrm{vdW}} = \sigma_{\mathrm{vdW}}h_e^3/D$, $\overline{\delta}_0 = \delta_0/h_e$, and $\overline{\Gamma} = 9\Gamma h_e^3/(2\delta_0 D)$. For the center-island and center-hole blisters, the van der Waals forces are included only in the regions interacting with the substrate underneath.

The Riks method is used to study the snap transitions of graphene blisters. The pressure p and the central deflection h are treated as two additional unknowns. The relationship between the central deflection and the angle of rotation requires that

$$\varphi_h(\boldsymbol{\theta}, \overline{h}) = \frac{\overline{a}}{n}\sum_{k=1}^{n-1}\theta_k + \overline{h} = 0 \tag{9}$$

To control the incremental arc length along the pressure-deflection curve, the pressure p can be related to the central deflection as

$$\varphi_p(\overline{p}, \overline{h}) = (\overline{p}-\overline{p}_{i-1})^2 + (\overline{h}-\overline{h}_{i-1})^2 - \Delta^2 = 0 \tag{10}$$

where Δ is specified as the dimensionless increment, and $\overline{p}_{i-1}$ and $\overline{h}_{i-1}$ are the normalized pressure and central deflection in the previous step. For computational efficiency, a regulated arc–length relation is used (except for the very first step):

$$\varphi_p'(\overline{p}, \overline{h}) = \left(\frac{\overline{p}-\overline{p}_{i-1}}{\overline{p}_{i-1}}\right)^2 + \left(\frac{\overline{h}-\overline{h}_{i-1}}{\overline{h}_{i-1}}\right)^2 - \Delta^2 = 0 \tag{11}$$

The Newton–Raphson method is employed to solve the system of nonlinear equations, including the discretized equilibrium equations and the two constraints in Eqs. (9) and (11). At each step, we start with a set of values as $\theta_k^{(0)}$, $\overline{u}_k^{(0)}$, $\overline{p}^{(0)}$, and $\overline{h}^{(0)}$, calculate the residual and corrections, and then iterate until a convergence condition is satisfied. At each iteration, a correction vector is calculated as

$$\begin{pmatrix} \Delta\boldsymbol{\theta} \\ \Delta\overline{\mathbf{u}} \\ \Delta\overline{p} \\ \Delta\overline{h} \end{pmatrix} = -\begin{bmatrix} \frac{\partial \mathbf{f}}{\partial \boldsymbol{\theta}} & \frac{\partial \mathbf{f}}{\partial \overline{\mathbf{u}}} & \frac{\partial \mathbf{f}}{\partial \overline{p}} & 0 \\ \frac{\partial \mathbf{g}}{\partial \boldsymbol{\theta}} & \frac{\partial \mathbf{g}}{\partial \overline{\mathbf{u}}} & 0 & 0 \\ \frac{\partial \varphi_h}{\partial \boldsymbol{\theta}} & 0 & 0 & \frac{\partial \varphi_h}{\partial \overline{h}} \\ 0 & 0 & \frac{\partial \varphi_p}{\partial \overline{p}} & \frac{\partial \varphi_p}{\partial \overline{h}} \end{bmatrix}^{-1} \begin{pmatrix} \mathbf{f} \\ \mathbf{g} \\ \varphi_h \\ \varphi_p \end{pmatrix} \tag{12}$$

where $\Delta\boldsymbol{\theta}$ is a vector of $n-1$ components ($\Delta\theta_k$, $k=1$ to $n-1$) and the same for $\Delta\overline{\mathbf{u}}$, $\boldsymbol{f}$, and $\boldsymbol{g}$. For the convergence criterion, we require that the L2-norm of the relative correction vector is smaller than a specified tolerance, namely,

$$|\mathbf{R}| = \left[\sum_{k=1}^{n-1}(\Delta\theta_k^2/\theta_k^2 + \Delta u_k^2/u_k^2)\right]^{1/2} < \tau \sim 10^{-4} \tag{13}$$

If not satisfied, the iteration procedure repeats with a new approximation, $\theta_k^{(i+1)} = \theta_k^{(i)} + \Delta\theta_k$, $\overline{u}_k^{(i+1)} = \overline{u}_k^{(i)} + \Delta\overline{u}_k$, $\overline{p}^{(i+1)} = \overline{p}^{(i)} + \Delta\overline{p}$, and $\overline{h}^{(i+1)} = \overline{h}^{(i)} + \Delta\overline{h}$.

4 Graphene Bubble Blisters

4.1 Nanobubble Blisters. Consider a nanobubble graphene blister with radius $a = 10\,\mathrm{nm}$ (Fig. 1(*a*)). Using the numerical method (Sec. 3) with $n = 300$, we calculate the blister deflection and central height versus the pressure, as shown in Fig. 3. Start with zero pressure and zero height. Subjected to increasing pressure, the central height increases until the pressure reaches a local maximum at point A (branch I). The slope of the pressure–height curve decreases and becomes zero at A, indicative of an impending instability under pressure control. Further increasing the pressure, a snap-through occurs from point A to point B along the horizontal dashed line, after which the height increases continuously (branch II). On the other hand, if the bubble blister starts with a height greater than point B on branch II and the pressure decreases, the unloading curve reaches a local minimum at point C, where the slope is again zero. Further decreasing the pressure would lead to a snap-back form point C to point D, returning to branch I. Hence, a snap-through/snap-back transition is predicted for the graphene bubble blister under the pressure-controlled loading and unloading. Between the two critical points (A and C), an

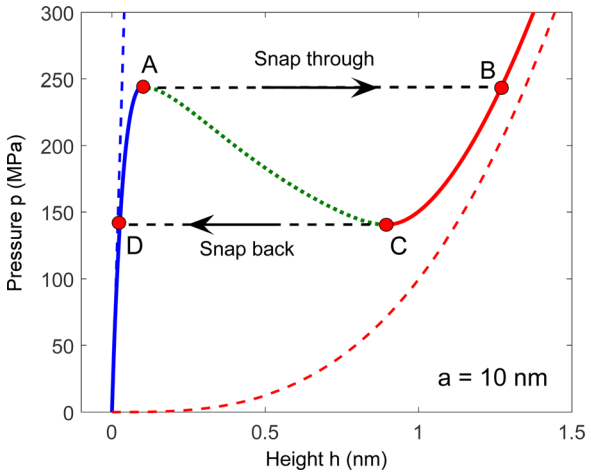

Fig. 3 Pressure versus height for a nanoscale graphene bubble blister ($a = 10$ nm), showing the snap transitions from A to B and from C to D. The dotted line is the unstable branch from A to C. The linear solution and the approximate membrane solution are shown as dashed lines for comparison.

unstable branch is obtained by the Riks method, where the height increases with decreasing pressure.

Figure 4 shows the snap-through/snap-back transitions of the deflection profile and corresponding van der Waals force distributions. We note that the deflection profiles take different shapes for the two stable branches: pancake-like at points A and D (branch I) and dome-like at points B and C (branch II). Correspondingly, the distributions of the van der Waals forces are different, nearly uniform for the pancake-like blister and concentrated near the edge for the dome-like blister. The two blister shapes can be analyzed approximately by a linearized model and a membrane model, as presented in the Appendix. The linearized model treats the van der Waals force as a linear spring so that the height increases linearly with the pressure, with a slope depending solely on the initial stiffness of the van der Waals interactions ($k_s = 27\Gamma/\delta_0^2$). As shown in Fig. 3, the linear solution agrees with the numerical solution when the height is small (branch I). On the other hand, the approximate membrane solution ignores the van der Waals forces and compares closely with the numerical solution when the height is relatively large (branch II). Bound by the two approximate solutions, the snap transitions in between can be understood from an energy consideration. As detailed in the Appendix, by using the two shape functions from the approximate solutions (Fig. 16) and minimizing the free energy of the system, the snap transitions can be predicted in good agreement with the numerical solution (Fig. 17).

The two critical pressures for the snap transitions can be determined numerically from the pressure–height curve as shown in Fig. 3, where the slope becomes zero ($dp/dh = 0$). Between the two critical pressures, the bubble blister is bistable, with two local minima for the free energy function. The state with the lower free energy is thermodynamically stable against any perturbation (not limited to small perturbations), while the other state is metastable. At a transition pressure ($p = p_t$), the two states have equal free energy. When $p < p_t$, the state on branch I (pancake-like blister) is thermodynamically stable; when $p > p_t$, the state on branch II (dome-like blister) is thermodynamically stable. Therefore, the snap transition of the graphene bubble blister is analogous to the first-order phase transition with a discontinuity in the central height (and volume). Similar snap transitions have been studied in other systems [35,36].

4.2 Microbubble Blisters. Next we consider microscale graphene bubble blisters, which are more commonly observed in experiments [11,12]. With the radius $a > 1\,\mu$m, the graphene membrane becomes highly flexible with increased nonlinearity

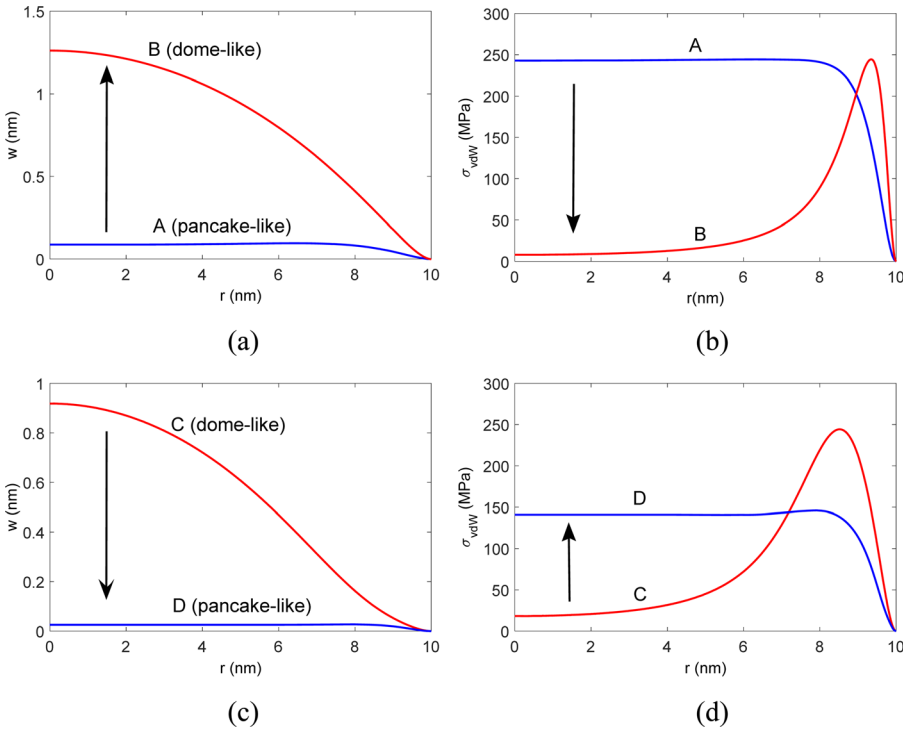

Fig. 4 Snap transitions of a nanoscale graphene bubble blister ($a = 10$ nm): (*a*) Snap-through of the deflection profile from A to B at $p = 243$ MPa; (*b*) distributions of the van der Waals force at A and B; (*c*) snap-back of the deflection profile from C to D at $p = 142$ MPa; and (*d*) distributions of the van der Waals force at C and D. The points A–D refer to those marked in Fig. 3.

due to relatively large deflections. Nevertheless, the problem can be solved by the same numerical method (Sec. 3) with a sufficiently large number of nodes (n). For $a = 1.5\,\mu$m, we found that using $n = 3000$ is sufficient to avoid numerical oscillations and the numerical results do not change noticeably with more nodes. Figure 5(*a*) shows the central height versus pressure, exhibiting similar snap transitions as the nanobubble blister in Fig. 3. The snap transitions are shown more clearly for the microbubble blister in a log–log plot (Fig. 5(*b*)), where the slope is close to 1 for branch I and about 3 for branch II, corresponding to the linear and membrane solutions, respectively. Moreover, we plot the volume of the blister versus pressure in Fig. 5(*c*). Interestingly, for the unstable branch, as the pressure decreases, the volume underneath the blister first decreases and then increases. Such a nonmonotonic behavior suggests that the blister would undergo snap transitions even if the loading/unloading is under strict volume control.

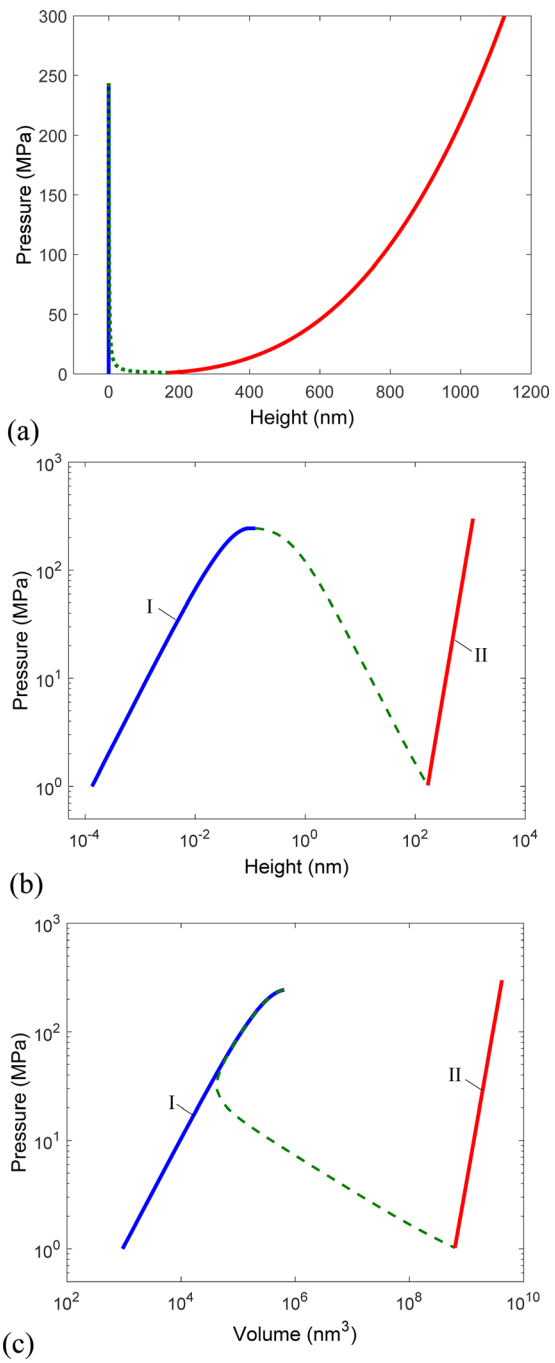

Fig. 5 (*a*) Pressure versus height for a microscale graphene bubble blister ($a = 1.5\,\mu$m). (*b*) Pressure–height in a log–log plot. (*c*) Pressure versus volume for the microbubble blister.

Figure 6 shows the deflection profiles of the microbubble blister. In the first stable branch of Fig. 5, the deflection is very small and almost uniform except near the edge (Figs. 6(*a*) and 6(*b*)). In this case, the pressure is largely balanced by the van der Waals forces. As the pressure increases, the deflection increases almost linearly. When the magnitude of the pressure becomes close to the strength of the van der Waals interactions ($\sigma_{\mathrm{vdW}}^{\max} = 1.466\Gamma/\delta_0$), the pancake-like blister becomes unstable with impending snap-through transition to a dome-like blister. Corresponding to the second stable branch in Fig. 5, the height of the dome-like blister decreases with decreasing pressure (Fig. 6(*f*)) until it becomes unstable and snaps back due to the presence of the attractive van der Waals forces. Along the unstable branch in Fig. 5, the center part of graphene membrane starts to bulge up at the point of snap-through transition, forming a dome-like shape while the rest part remains flat (Figs. 6(*c*) and 6(*d*)). Such a deflection profile may be considered as a mixture of two states, dome-like center surrounded by a pancake-like annulus. The bulge expands in the radial direction with increasing central height and decreasing pressure (Fig. 6(*e*)), similar to growth of a bubble blister with interfacial delamination. The unstable branch terminates at the point of snap-back transition, when the bulge radius reaches the prescribed bubble radius. In this section, we assume the bubble radius to be fixed. The growth of the bubble radius is considered in Sec. 6.

Notably, while the critical pressures for snap-through (from pancake-like to dome-like) are similar for both nano- and microbubble blisters, the critical pressure for snap-back (from dome-like to pancake-like) is much lower for the microbubble blister. It is found that the snap-through pressure approximately equals the strength of the van der Waals interactions, i.e., $p_{\mathrm{st}} \sim \sigma_{\mathrm{vdW}}^{\max} = 1.466\Gamma/\delta_0$, at a height close to $0.165\delta_0$ ($\sim$0.1 nm), both insensitive to the blister radius (Fig. 7). On the other hand, the snap-back pressure depends sensitively on the blister radius, decreasing with increasing blister radius, as shown in Fig. 7(*a*). Meanwhile, the snap-back height increases almost linearly with increasing blister radius (Fig. 7(*b*)). The linear dependence may be expected from the approximate membrane solution [20], which predicts $h \propto a$ for a given adhesion energy. Further, by the membrane solution in Eq. (A7), $p \propto a^{-4}h^3$, and thus the critical pressure for snap-back is inversely proportional to the radius (i.e., $p_{\mathrm{sb}} \propto a^{-1}$). Moreover, by an energy consideration, the snap-back pressure depends on the adhesion energy as $p_{\mathrm{sb}} \propto \Gamma^{3/4}$ and correspondingly the snap-back height, $h_{\mathrm{sb}} \propto \Gamma^{1/4}$. It should be noted that the approximate membrane solution becomes less accurate for nanobubble blisters [21]. With the two critical pressures for the snap transitions and the corresponding heights, two phase diagrams are constructed in Fig. 7 for the graphene bubble blisters. On the pressure–radius panel (Fig. 7(*a*)), a bistable region is identified between the two critical pressures. On the height–radius panel (Fig. 7(*b*)), an unstable region is identified between the two critical heights.

Dome-like graphene bubbles are commonly observed in experiments [11,12], whereas the pancake-like bubbles are difficult to observe because of very small height ($h < 1$ nm). For dome-like microbubbles ($a > 1\,\mu$m), the approximate membrane solution may be used to estimate the adhesion energy of graphene from measurements of the bubble radius and height [20]: $\Gamma = 5E_{2D}h^4/8\phi(\nu)a^4$. To determine the other parameter of van der Waals interactions (i.e., δ_0), additional measurements are required. For a fixed graphene bubble radius, measurement of the critical pressure for the snap-through transition would be sufficient to deduce the second parameter as $p_{\mathrm{st}} \sim \sigma_{\mathrm{vdW}}^{\max} = 1.466\Gamma/\delta_0$. However, it remains a challenge to design such an experiment. Instead, the center-island blister test is more suitable for this purpose, as discussed in Sec. 5.

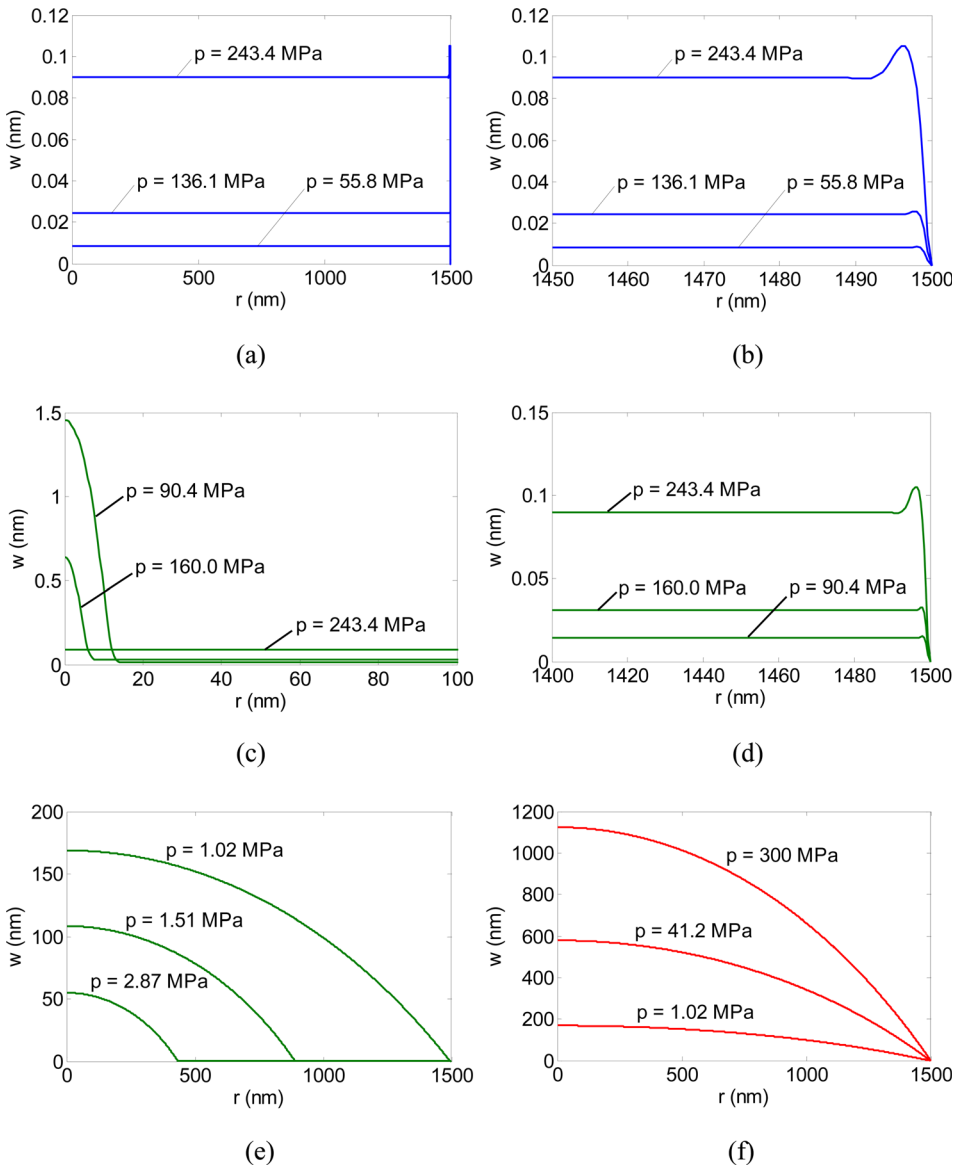

Fig. 6 Evolution of deflection profile for a microscale graphene bubble blister ($a = 1.5\ \mu$m): (*a*) and (*b*) for increasing pressure along branch I (stable), with (*b*) showing the deflection near the edge; (*c*)–(*e*) for decreasing pressure along the unstable branch, with (*c*) showing the deflection near the center and (*d*) showing the deflection near the edge; (*f*) for increasing pressure along branch II (stable)

5 Center-Island Graphene Blisters

Island blister tests have been used to measure the adhesion properties of thin films or membrane materials to their substrates [1,3]. As illustrated in Fig. 1(*b*), we consider a circular hole of radius $a = 1.5\ \mu$m with a circular island of radius $b = 0.25\ \mu$m at the center. This configuration is similar to those used in experiments for graphene [9,10]. Here, the van der Waals forces are considered only for the center part of the graphene with $0 < r < b$. Figure 8 shows the numerical results in terms of the center height versus pressure and the blister volume versus pressure. The blister volume is calculated by integrating the deflection profile, without including the volume of the hole. Similar to the graphene bubble blisters, three branches are obtained, two stable branches and an unstable branch in between. Hence, snap transitions between the two stable branches are predicted during both pressurization and depressurization. The deflection profiles are presented in Fig. 9. For a relative low pressure, the center deflection is nearly zero due to the presence of van der Waals forces between graphene and the island, whereas the graphene around the island deflects, forming a donut-like shape (Fig. 9(*a*)). The central height increases linearly with increasing pressure until it reaches the point of snap-through transition. Along the unstable branch, the deflection profiles in Figs. 9(*b*) and 9(*c*) show an unstable delamination and popping process: starting from the edge of the island, the graphene delaminates progressively from the substrate and pops up as the pressure continues decreasing. The center deflection remains nearly zero before the graphene is fully delaminated from the island, thus making this part of the unstable branch indistinguishable from the first stable branch in Fig. 8(*a*). However, the volume underneath the blister is distinguishable, as shown in Fig. 8(*b*). The unstable branch terminates at the point of snap-back transition, beyond which the central height increases with increasing pressure and the blister takes a dome-like shape (Fig. 9(*d*)). Therefore, in this case, the snap-through transition is from a donut-like blister to a dome-like blister and vice versa for the snap-back transition.

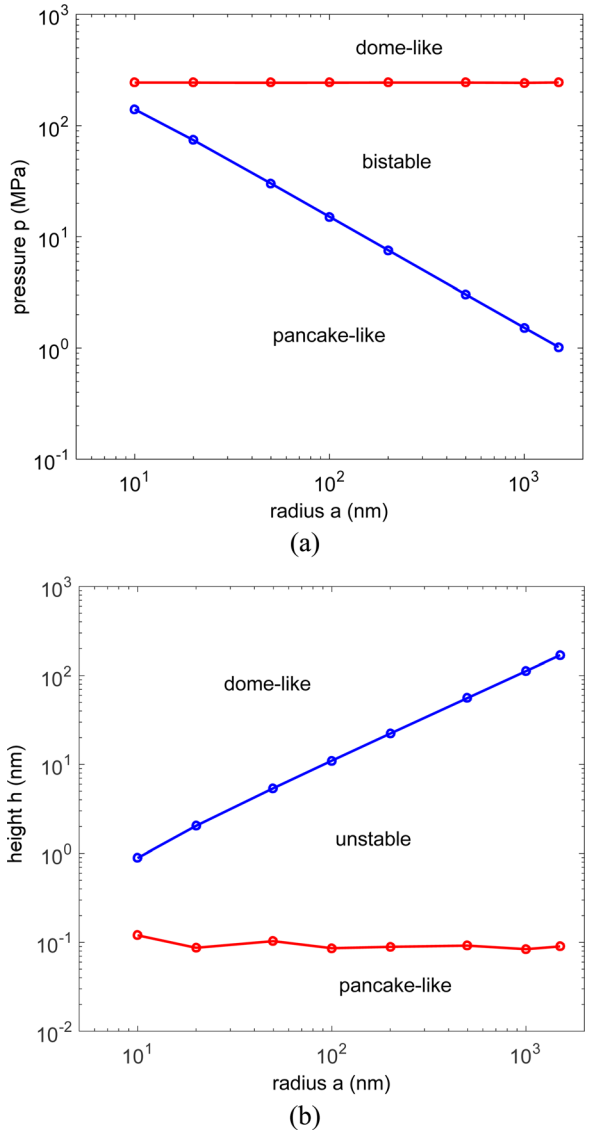

Fig. 7 Phase diagrams for graphene bubble blisters: (*a*) pressure versus radius and (*b*) height versus radius

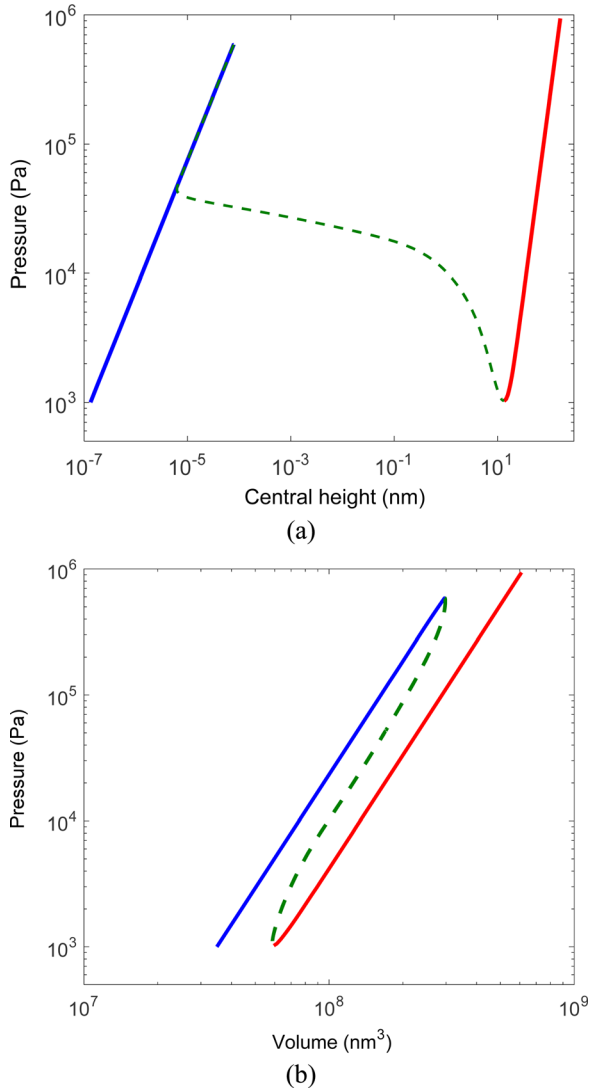

Fig. 8 (*a*) Central height versus pressure and (*b*) volume versus pressure for a center-island graphene blister ($a = 1.5\,\mu$m and $b = 0.25\,\mu$m)

Moreover, Fig. 8(*b*) shows that the snap transitions are expected under both pressure and volume control.

With the center-island configuration, it is possible to determine both parameters (adhesion energy Γ and equilibrium separation δ_0) for the van der Waals interactions between graphene and the substrate by measuring the critical pressures for the snap-through and snap-back transitions [9,10]. For a fixed blister size (a and b), the critical pressure for snap-through depends primarily on the adhesion energy, while the critical pressure for snap-back depends on a combination of the two parameters. First, for the snap-back transition, we note in Fig. 9(*d*) that the separation between graphene and the surface of the center island is over 10 nm, much larger than the typically expected range for van der Waals interactions (<3 nm). At such a large separation, the van der Waals interactions can be simplified by ignoring the second term in Eq. (3), which is for the short-ranged repulsion. With $w \gg \delta_0$, the traction is approximately

$$\sigma_{\mathrm{vdW}}(w) \approx \beta w^{-4} \tag{14}$$

where $\beta = (9/2)\Gamma\delta_0^3$ is the single parameter combining the effects of Γ and δ_0. As a result, the critical pressure for the snap-back transition depends on the interactions through the combined parameter β. The corresponding pull-in distance (i.e., the central height at the point of snap-back) also depends on β. As shown in Fig. 10, by varying both Γ and δ_0, we obtain the critical pressure and pull-in distance as functions of β. The results for different values of Γ collapse onto a master curve with only dependence on β. Therefore, a measurement of the critical pressure or the pull-in distance would determine the value of β as a combination of the two parameters (Γ and δ_0).

The snap-through transition occurs as the graphene delaminates from the center island. As shown in Fig. 9(*b*), the delamination starts from the edge of the island and grows toward the center. Under pressure control, the delamination growth is unstable and snaps through upon initiation. By a fracture mechanics consideration, assuming small-scale bridging, the critical pressure for the snap-through transition would depend on the adhesion energy Γ only. As outlined in the Appendix, an approximate membrane analysis predicts the critical pressure as $p_c = \eta E_{2D}^{1/4}\Gamma^{3/4}a^{-1}$, which is compared to the numerical results in Fig. 11. The numerical results for three different values of δ_0 are nearly identical, in very good agreement with the membrane analysis. Therefore, the adhesion energy Γ can be determined by measuring the critical pressure for snap-through transition using the center-island blister configuration. Together with measurement of the critical pressure

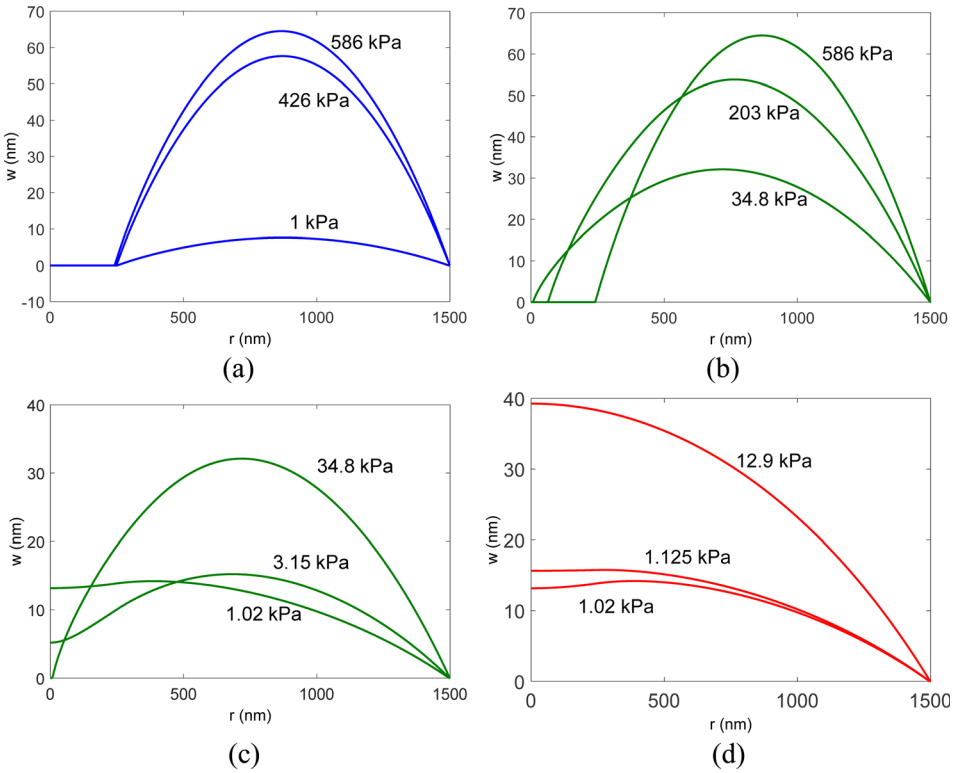

Fig. 9 Deflection profiles of a center-island graphene blister ($a = 1.5\,\mu$m and $b = 0.25\,\mu$m): (*a*) donut-like profiles (stable branch I), (*b*) and (*c*) delamination and popping (unstable branch), and (*d*) dome-like profiles (stable branch II)

for snap-back or the pull-in distance, both parameters (Γ and δ_0) for the van der Waals interactions can be determined.

In their experiments, Liu et al. [9] measured pull-in distances for center-island graphene blisters, ranging from 8 nm to 10 nm for monolayer graphene. Taking 9.2 nm as the pull-in distance, we obtain from Fig. 10(*b*) $\beta = 0.0083$ nN nm^2. In subsequent experiments, Boddeti et al. [10] measured the critical pressure for snap-through to be around 1 MPa, although the island dimension is slightly different ($b = 0.35$ nm). Based on these two measurements, we obtain $\Gamma = 0.2$ J/m^2 and $\delta_0 = 0.21$ nm. Both of these values appear to be lower than expected. As noted by Liu et al. [9], the graphene membranes may have been subjected to a pretension ($\sim$0.07 N/m), and the effects of pretension could be significant for both snap-back and snap-through transitions.

An analytical model was presented by Liu et al. [9] for the snap-back transition, assuming uniform attraction and negligible bending stiffness of graphene. As shown in Fig. 10, the analytical model (with zero pretension) overestimates the pull-in distance compared to the numerical results, while the critical pressure agrees closely with the numerical results. For the snap-through transition, an analytical model was also presented by Boddeti et al. [10], assuming a uniform radial tension and negligible circumferential strain in graphene. The predicted critical pressure has the same scaling as our analysis, i.e., $p_c \sim E_{2D}^{1/4}\Gamma^{3/4}a^{-1}$, but slightly lower than the numerical results as shown in Fig. 11.

6 Center-Hole Graphene Blisters

Center-hole blisters are the standard configuration commonly used in experiments under either pressure- or volume-controlled condition [4,8]. The gas impermeability of graphene allowed blister tests under the condition of N-control [6,7], where N refers to the number of trapped gas molecules. As illustrated in Fig. 1(*c*), we consider a circular hole of radius $b = 0.25\,\mu$m, with which the graphene blister is pressurized and the radius of the blister may grow by delamination from the substrate. The outer radius a is set to be 1.5 μm to stop the delamination. In this case, van der Waals interactions are considered only for the annular region ($a > r > b$). Figure 12(*a*) shows the calculated pressure–volume curve for the graphene blister. For the first segment (A to B), the blister radius remains constant and the pressure increases with volume. The approximate membrane analysis predicts that $p \propto V^3$ for a fixed blister radius [20], in good agreement with the numerical results. For the second segment (B to C), the pressure decreases and the volume increases, due to increasing blister radius. Again, by the membrane analysis, $p \propto V^{-1/3}$ is predicted for a constant energy release rate (equal to the adhesion energy). Finally, for the third segment (C to D), the blister radius is fixed at the prescribed outer radius a, and the pressure increases with volume as $p \propto V^3$. Evidently, the p–V curve of the graphene blister confirms that the growth of the blister is unstable under a pressure control but stable under a volume control. Under the N-control, we assume $pV = NkT$ by the ideal gas law, where k is the Boltzmann constant and T is temperature. As shown in Fig. 12(*a*), the p–V curve of the ideal gas intersects the p–V curve of the graphene blister, giving the equilibrium solution under the condition of N-control. Notably, for each value of N, only one intersection can be found, indicating stable growth of the graphene blister under the N-controlled condition.

The equilibrium deflection profiles of the center-hole graphene blister are shown in Fig. 12(*b*) for increasing N. The central height, the pressure, and the blister radius are shown in Fig. 13 as functions of N. The numerical results are compared to the predictions by the approximate membrane analysis [20]. First, for the blister with a fixed radius (b), the central height can be obtained from Eq. (A7) in conjunction with the ideal gas law:

$$h = \left[\frac{2\phi(\nu)}{\pi}\right]^{1/4} E_{2D}^{-1/4} b^{1/2} (NkT)^{1/4} \tag{15}$$

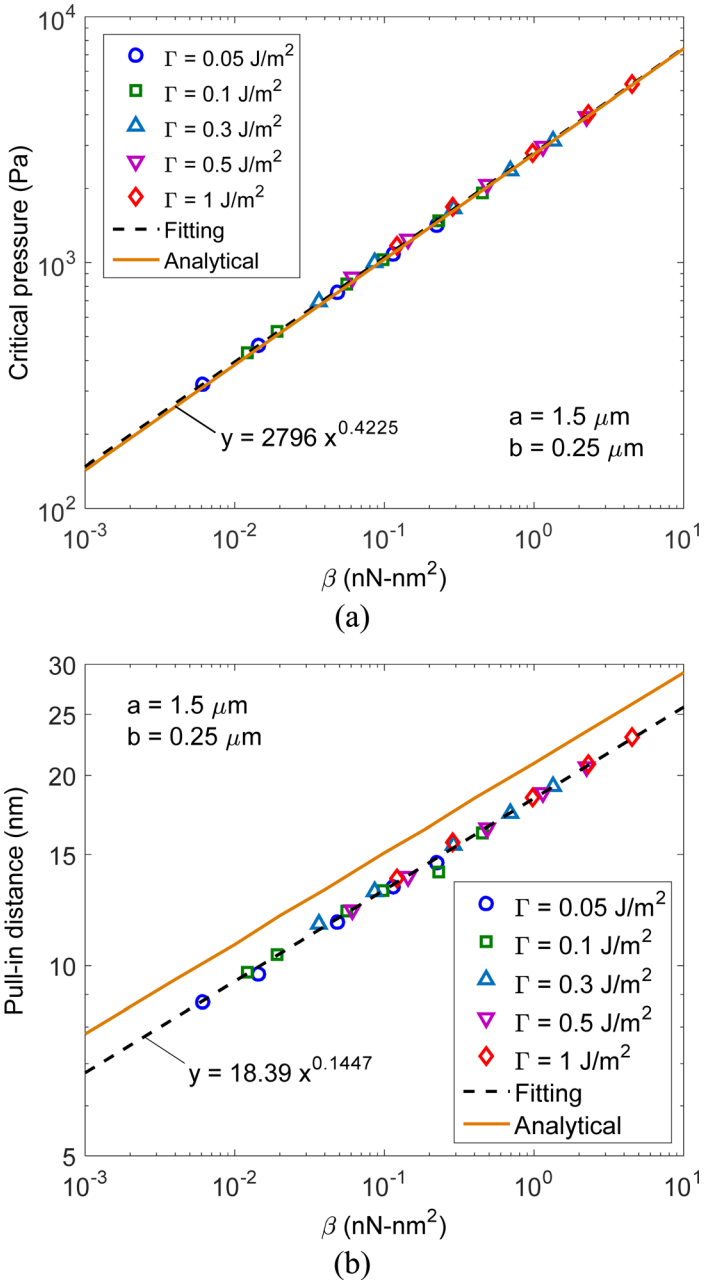

Fig. 10 Snap-back transition for a center-island graphene blister ($a = 1.5\,\mu$m and $b = 0.25\,\mu$m): (*a*) critical pressure and (*b*) pull-in distance. The analytical solutions from Liu et al. [9] are shown for comparison.

Correspondingly, the pressure is

$$p = \left[\frac{8}{\pi^3\phi(\nu)}\right]^{1/4} E_{2D}^{1/4} b^{-5/2} (NkT)^{3/4} \tag{16}$$

Next, for a constant energy release rate (equal to the adhesion energy Γ), we obtain by the membrane analysis:

$$h = \left(\frac{5\phi(\nu)}{2\pi^2}\right)^{1/4} (E_{2D}\Gamma)^{-1/4} (NkT)^{1/2} \tag{17}$$

and

$$p = \left[\frac{2^{13}\pi^2}{5^5\phi(\nu)}\right]^{1/4} E_{2D}^{1/4} \Gamma^{5/4} (NkT)^{-1/2} \tag{18}$$

The growth of the blister radius is predicted as

$$\Delta b = \left(\frac{5}{4\pi}\right)^{1/2} \Gamma^{-1/2} (NkT)^{1/2} - b \tag{19}$$

where N is assumed to be greater than the critical value, $N_C = 4\pi b^2\Gamma/(5kT)$. These predictions are in reasonable agreement with the numerical results. The discrepancy is most likely

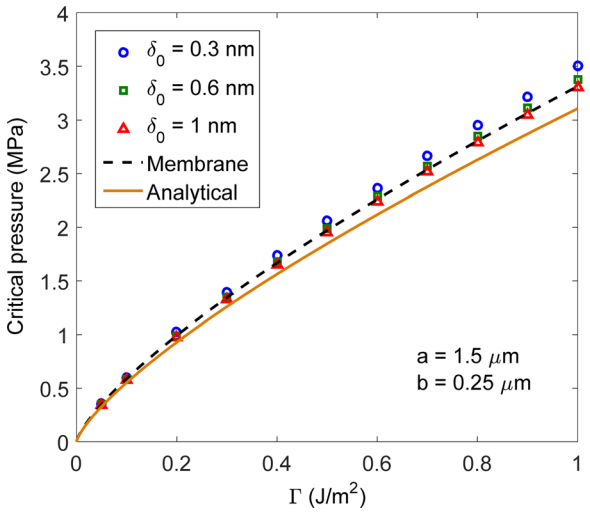

Fig. 11 Critical pressure for snap-through transition of a center-island graphene blister ($a = 1.5\,\mu$m and $b = 0.25\,\mu$m), as a function of the adhesion energy Γ. The predictions by the membrane analysis in the Appendix and the analytical model in Boddeti et al. [10] are shown in comparison with the numerical results (symbols).

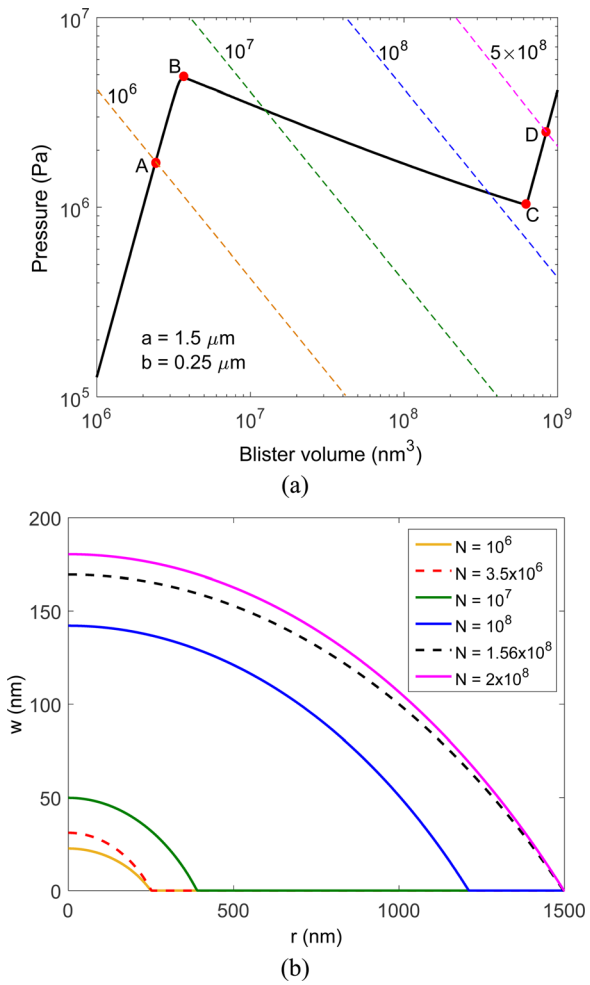

Fig. 12 (*a*) Pressure–volume curve for a center-hole graphene blister ($a = 1.5\,\mu$m and $b = 0.25\,\mu$m). The dashed lines correspond to the ideal gas law, $pV = NkT$, with different values of N as indicated ($T = 300$ K). (*b*) Deflection profiles for increasing number of gas molecules. The dashed lines correspond to the critical points B and C in (*a*).

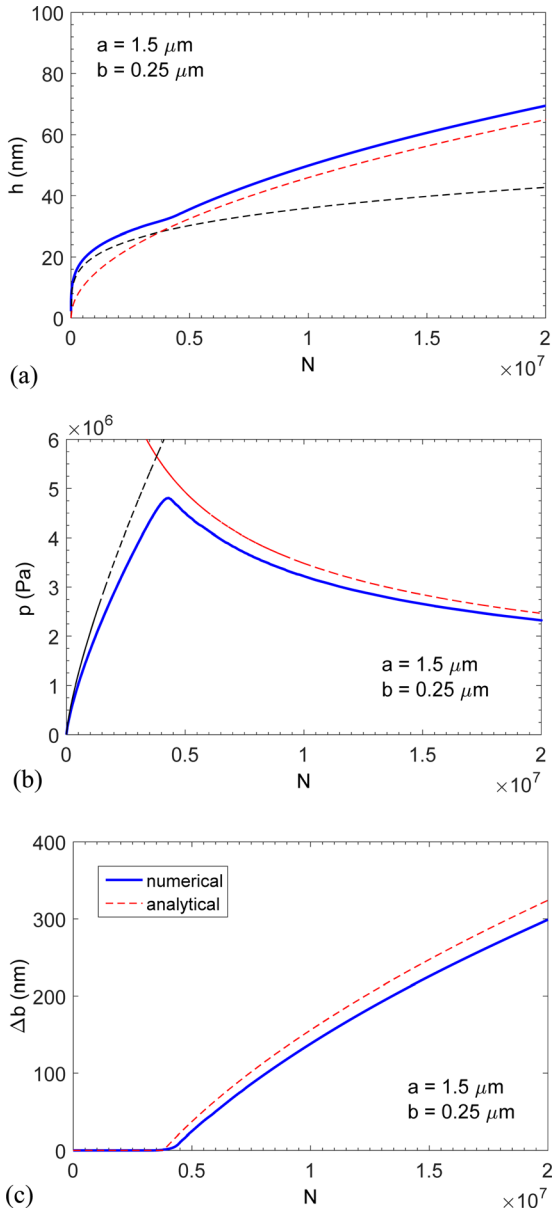

Fig. 13 (*a*) Central height, (*b*) pressure, and (*c*) the change of radius for a center-hole graphene blister ($a = 1.5\,\mu$m and $b = 0.25\,\mu$m). Dashed lines show the predictions by the approximate membrane analysis.

due to the approximate shape function used in the membrane analysis. A more accurate (also more complicated) shape function was used in Hencky's membrane analysis [37], which would lead to similar predictions except for the coefficient $\phi(\nu)$ and a constant shape factor for the volume. As noted in the previous studies [20,21], the difference between the two membrane analyses is fairly small.

The presence of van der Waals interactions leads to a cohesive zone near the edge of the graphene blister. It is found that the size of the cohesive zone is relatively small ($\sim$5 nm), but depending on the two parameters (Γ and δ_0) used for the van der Waals interactions. In experiments, the two parameters may be determined by measuring the delamination resistance curve (R-curve) of the center-hole blister [29]. By measuring the blister height and radius, the energy release rate for delamination may be calculated based on the approximate membrane analysis [20]: $G = 5E_{2D}h^4/[8\phi(\nu)a^4]$. Alternatively, if the pressure can be measured, we may calculate the energy release rate as $G = 5ph/8$. By

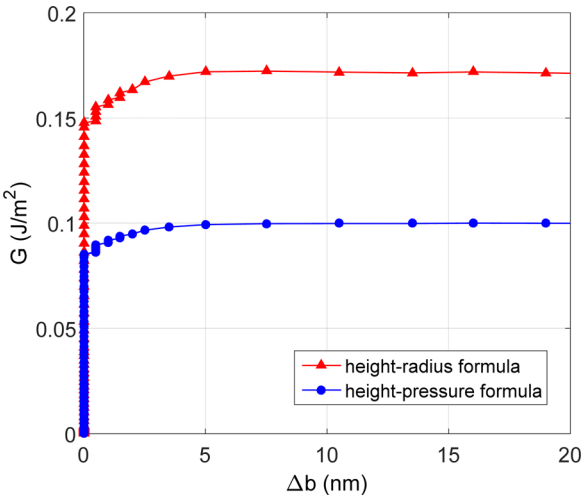

Fig. 14 Calculated delamination resistance curves for a center-hole graphene blister ($a = 1.5\ \mu$m and $b = 0.25\ \mu$m) using two different formulas based on the approximate membrane analysis

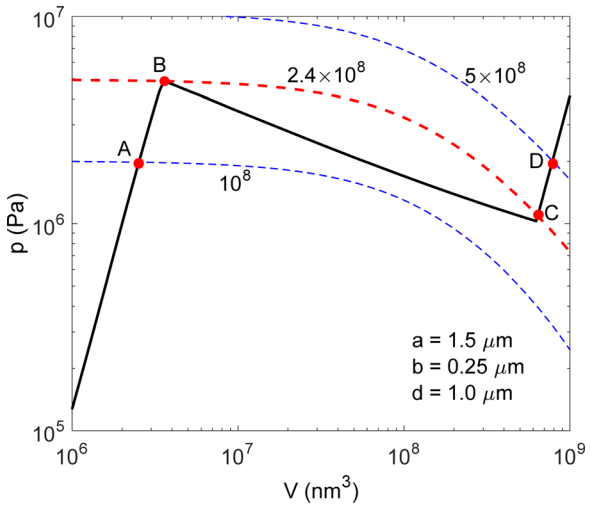

Fig. 15 Pressure–volume curves, (*a*) for unstable growth of a center-hole graphene blister ($d = 1.0\ \mu$m) and (*b*) for stable growth with $d = 0.01\ \mu$m, both under *N*-control. The dashed lines correspond to the ideal gas law with different values of *N* as indicated ($T = 300$ K).

the numerical method, we calculate the *R*-curve as shown in Fig. 14. Using the height–pressure formula, the *R*-curve saturates at the prescribed adhesion energy ($\Gamma = 0.1\ \text{J/m}^2$) for $\Delta b > 5$ nm. The height–radius formula, however, overestimates the adhesion energy. The shape of the *R*-curve depends on the traction–separation relation, which in this case depends on the equilibrium separation δ_0. Hence, both parameters (Γ and δ_0) may be determined from the *R*-curve if it can be measured with sufficient accuracy.

In their experiments, Koenig et al. [6] measured the height and radius of pressurized graphene blisters in a center-hole configuration. They calculated the equilibrium pressure by assuming the ideal gas law for a constant number of trapped gas molecules, with which they determined the adhesion energy of graphene based on Hencky's membrane analysis. More interestingly, in a subsequent study, Boddeti et al. [7] noticed that the initial growth of the graphene blister may be either stable or unstable, depending on the depth of the hole. The stability of the blister growth may be understood based on the *p*–*V* curves (Fig. 12(*a*)). With a finite depth (d) for the hole and a constant outer pressure (p_{out}), the ideal gas law may be written as

$$(p + p_{\text{out}})(V + \pi b^2 d) = NkT \tag{20}$$

Taking $p_{\text{out}} = 0.1$ MPa as the outer pressure, we plot the *p*–*V* curves for two different depths in Fig. 15. The *p*–*V* curve for the blister is the same as that in Fig. 12(*a*), but the *p*–*V* curves for the trapped gas depend on the hole depth (d). For a relatively deep hole ($d = 1\ \mu$m in Fig. 15(*a*)), multiple intersections become possible for some values of *N*, giving multiple solutions. This is similar to the pressure-controlled scenario, which may be considered as an extreme case with $d \to \infty$. In particular, as illustrated in Fig. 15(*a*), a snap transition from point B to point C is predicted for the graphene blister subjected to increasing *N*. On the other hand, for a shallow hole ($d = 0.01\ \mu$m in Fig. 15(*b*)), each *p*–*V* curve of the trapped gas has only one intersection with the *p*–*V* curve of the blister, similar to the case in Fig. 12(*a*) where $d = 0$ is implied. In this case, the blister would grow stably and continuously from B to C. Therefore, by varying the hole depth, both stable and unstable growth may be achieved with the center-hole blister configuration.

7 Summary

This paper presents a numerical study on snap transitions of pressurized graphene blisters. A continuum model is adopted combining a nonlinear plate theory for monolayer graphene with a nonlinear traction–separation relation for van der Waals interactions between graphene and the substrate. A numerical method is developed to solve the nonlinear problem with snap transitions. Three types of blister configurations are considered. For graphene bubble blisters, snap-through and snap-back transitions between pancake-like and dome-like shapes are predicted under the pressure-controlled condition. Phase diagrams are constructed for nano- to microscale bubble blisters, with bistable and unstable regions identified for the pressure and height, respectively. For center-island graphene blisters, snap transitions between donut-like and dome-like shapes are predicted under both pressure and volume control. Finally, for the center-hole graphene blisters, unstable growth is expected under pressure control, but stable growth is predicted under the volume or *N*-control. With a finite hole depth, however, the growth may start with a snap transition (unstable growth) under *N*-control if the hole is relatively deep.

The numerical results provide a systematic understanding on the mechanics of graphene blisters, consistent with previously reported experiments. Of particular interest is the relationship between the van der Waals interactions and measurable quantities in corresponding blister tests. As a result, the adhesion energy of graphene may be determined from measurements of the radius and height of graphene bubble blisters. Both the adhesion energy

and the equilibrium separation for the van der Waals interactions can be determined from measurements of the critical pressures (or critical separation) for snap-back and snap-through transitions of the center-island graphene blisters. With the standard center-hole blister configuration, measurement of the delamination resistance curve could provide sufficient information for the traction–separation relation of the interface. It is noted that, while an approximate membrane analysis may be used in most cases (especially for relatively large blisters), some quantitative discrepancies between the analytical and numerical results do exist. The more accurate numerical solutions may be used in conjunction with experiments for quantitative characterization of the interfacial properties of graphene as well as other 2D membrane materials. Moreover, the numerical method may also be used to explore potential applications of the graphene blisters such as strain engineering and nano-electromechanical devices.

Appendix

A Linear Solution for Graphene Bubble Blisters. For very small deflection, we linearize the van der Waals force in Eq. (3) as

$$\sigma_{\text{vdW}} \approx k_s w \tag{A1}$$

where $k_s = 27\Gamma/\delta_0^2$ is the initial stiffness. Moreover, the equilibrium equations are linearized to recover the linear plate equation for the deflection:

$$\frac{D}{r}\frac{d}{dr}\left(r\frac{d^3w}{dr^3}+\frac{d^2w}{dr^2}-\frac{1}{r}\frac{dw}{dr}\right) = p - k_s w \tag{A2}$$

which is identical to the problem of a linear plate resting on an elastic foundation. Solving Eq. (A2), the deflection profile is obtained as

$$w(r) = \frac{p}{k_s}N_1(r) \tag{A3}$$

where the shape function is

$$N_1(r) = 1 - \frac{\xi_2 J_1(\xi_2 a)J_0(\xi_1 r) - \xi_1 J_1(\xi_1 a)J_0(\xi_2 r)}{\xi_2 J_1(\xi_2 a)J_0(\xi_1 a) - \xi_1 J_1(\xi_1 a)J_0(\xi_2 a)} \tag{A4}$$

with $\xi_1 = \sqrt{2}(1+i)/2(k_s/D)^{1/4}$ and $\xi_2 = \sqrt{2}(1-i)/2(k_s/D)^{1/4}$. A length scale for the shape function emerges: $L_1 = (D/k_s)^{1/4}$, which is about 0.4 nm for monolayer graphene. As shown in Fig. 16, this shape function is a constant except in the annular region near the edge of the blister. In this case, the shape of the blister is pancake-like and the central height depends on the pressure linearly as $h = p/k_s$. Hence, the initial slope of the pressure–height curve (Fig. 3) is directly related to the stiffness of van der Waals interactions.

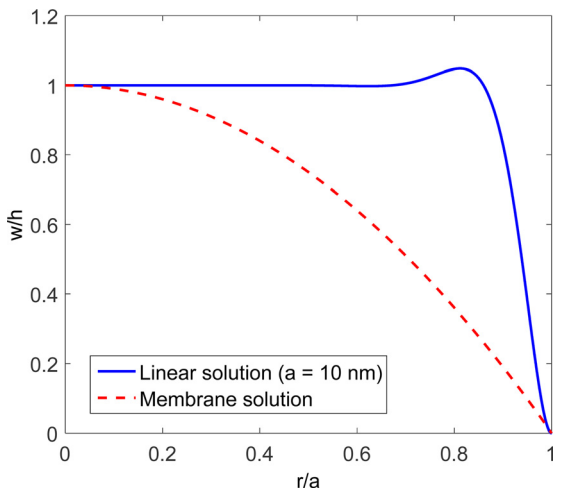

Fig. 16 Shape functions for graphene bubble blisters

A Membrane Solution for Graphene Bubble Blisters. By neglecting the van der Waals forces ($\sigma_{\text{vdW}} \approx 0$), an approximate membrane solution was obtained in a previous study [20], with a deflection profile

$$w(r) = hN_2(r) \tag{A5}$$

where the shape function is

$$N_2(r) = 1 - \frac{r^2}{a^2} \tag{A6}$$

and the central deflection is related to the pressure as

$$h = [\phi(\nu)pa^4/E_{2D}]^{1/3} \tag{A7}$$

with $\phi(\nu) = 75(1-\nu^2)/[8(23+18\nu-3\nu^2)]$. As shown in Fig. 16, the shape of the blister in this case is dome-like.

A Two-State Solution for Graphene Bubble Blisters. By combining the two shape functions from the linear solution and the membrane solution, an approximate deflection profile may be written as

$$w(r) = h_1 N_1(r) + h_2 N_2(r) \tag{A8}$$

where h_1 and h_2 are to be determined. Correspondingly, the radial displacement is

$$u(r) = \frac{2(3-\nu)h_2^2}{5a}\frac{r}{a}\left(1-\frac{r}{a}\right) \tag{A9}$$

which is part of the membrane solution [20].

The total free energy of the blister includes the elastic strain energy of graphene, the van der Waals interaction energy, and the potential energy associated with the pressure, namely,

$$\Phi(h_1,h_2;p,a) = 2\pi\int_0^a [U_b(r)+U_s(r)+U_{\text{vdw}}(r)]rdr - 2\pi p\int_0^a w(r)rdr \tag{A10}$$

where the van der Waals interaction energy is [27]

$$U_{\text{vdw}}(r) = -\Gamma\left[\frac{3}{2}\left(\frac{\delta_0}{\delta_0+w}\right)^3 - \frac{1}{2}\left(\frac{\delta_0}{\delta_0+w}\right)^9\right] \tag{A11}$$

and the elastic energy due to stretching and bending of graphene are, respectively,

$$U_b(r) = \frac{D}{2}\left(\left(\frac{d^2w}{dr^2}\right)^2 + \frac{1}{r^2}\left(\frac{dw}{dr}\right)^2 + \frac{2}{r}\frac{D-D_G}{D}\frac{dw}{dr}\frac{d^2w}{dr^2}\right) \tag{A12}$$

$$U_s(r) = \frac{E_{2D}}{2(1-\nu^2)}\left(\varepsilon_r^2 + 2\nu\varepsilon_r\varepsilon_\theta + \varepsilon_\theta^2\right) \tag{A13}$$

Note that the bending energy in Eq. (A12) includes a term related to Gaussian curvature with a Gaussian curvature modulus D_G. However, it can be shown that the Gaussian curvature term drops out after integration over the area with the clamped boundary

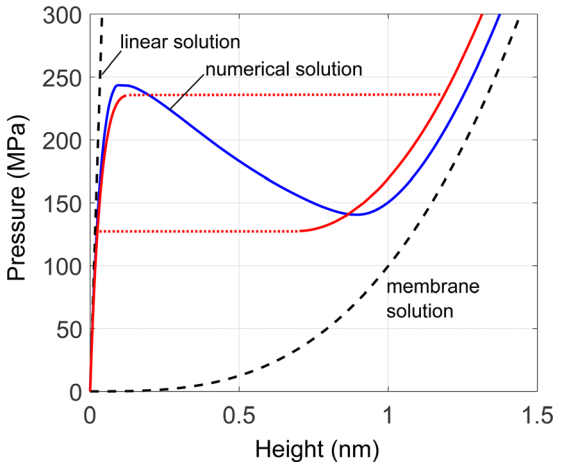

Fig. 17 Comparison of the approximate two-state solution by energy minimization with the numerical solution for the pressure–height curve of a graphene bubble blister ($a = 10$ nm)

condition and hence has no influence on the result. In Eq. (A13), the strain components are related to the displacements as usual: $\varepsilon_r = du/dr + 1/2(dw/dr)^2$ and $\varepsilon_\theta = u/r$.

For a given radius a and pressure p, we minimize the free energy in Eq. (A10) to determine the coefficients h_1 and h_2. The central height of the blister is then simply $h = h_1 + h_2$. For $a = 10$ nm, as shown in Fig. 17, the result from energy minimization is in reasonable agreement with the numerical solution. Under a small pressure (e.g., $p = 100$ MPa), the free energy has only one minimum corresponding to a state of small deflection with a pancake-like shape. As the pressure increases (e.g., $p = 200$ MPa), two local minima appear in the energy landscape along with a saddle point in between. The two minima correspond to the two stable branches in the pressure–height curve, while the saddle point corresponds to the unstable branch. When p increases further (e.g., $p = 300$ MPa), the first local minimum disappears and the remaining minimum corresponds to branch II with a dome-like deflection profile. Thus, the snap transitions of the bubble blister can be understood as a result of energy minimization. In particular, the competition between the van der Waals interaction energy and the elastic energy of graphene leads to the two states with different blister shapes.

A Membrane Analysis for Center-Island Graphene Blisters. For the center-island blister, we assume a deflection profile (before snap-through)

$$w(r) = \begin{cases} 0, & 0 \le r < b \\ h\left[1 - \left(\dfrac{r - \dfrac{a+b}{2}}{\dfrac{a-b}{2}}\right)^2\right], & b \le r \le a \end{cases} \tag{A14}$$

where h is the maximum deflection. In addition, for the deformation to be kinematically admissible, a radial displacement is assumed

$$u(r) = \begin{cases} 0, & 0 \le r < b \\ u_0 \dfrac{r-b}{a-b}\left[1 - \dfrac{r-b}{a-b}\right], & b \le r \le a \end{cases} \tag{A15}$$

where u_0 is a parameter to be determined.

Following the energy minimization method in Ref. [20], the total potential energy of the graphene blister is written as a function of the kinematic parameters: $\Pi = \Pi(h, u_0; a, b, p)$. Then, for given a, b, and p, the equilibrium values of h and u_0 are obtained by minimizing the potential energy: $\partial\Pi/\partial h = \partial\Pi/\partial u_0 = 0$. It is found that the height scales with the pressure as $h \sim p^{1/3}$.

For the graphene to delaminate from the center island, the release of the potential energy must exceed the adhesion energy. Therefore, the critical condition is set up as

$$\left(\frac{\partial\Pi}{\partial b}\right)_p = 2\pi b\Gamma \tag{A16}$$

which predicts a critical pressure as a function of the adhesion energy as $p_c = \eta E_{2D}^{1/4}\Gamma^{3/4}a^{-1}$ and η is a dimensionless coefficient depending on the ratio b/a. For $a = 1.5\,\mu$m and $b = 0.25\,\mu$m, we obtain $\eta = 1.392$.

References

[1] Allen, M. G., and Senturia, S. D., 1989, "Application of the Island Blister Test for Thin Film Adhesion Measurement," J. Adhes., **29**(1–4), pp. 219–231.
[2] Jensen, H. M., 1991, "The Blister Test for Interface Toughness Measurement," Eng. Fract. Mech., **40**(3), pp. 475–486.
[3] Lai, Y. H., and Dillard, D. A., 1994, "A Study of the Fracture Efficiency Parameter Blister Tests for Films and Coatings," J. Adhes. Sci. Technol., **8**(6), pp. 663–678.
[4] Xu, D., and Liechti, K. M., 2010, "Bulge Testing Transparent Thin Films With Moiré Deflectometry," Exp. Mech., **50**(2), pp. 217–225.
[5] Zong, Z., Chen, C. L., Dokmeci, M. R., and Wan, K. T., 2010, "Direct Measurement of Graphene Adhesion on Silicon Surface by Intercalation of Nanoparticles," J. Appl. Phys., **107**(2), p. 026104.
[6] Koenig, S. P., Boddeti, N. G., Dunn, M. L., and Bunch, J. S., 2011, "Ultrastrong Adhesion of Graphene Membranes," Nat. Nanotechnol., **6**(9), pp. 543–546.
[7] Boddeti, N. G., Koenig, S. P., Long, R., Xiao, J., Bunch, J. S., and Dunn, M. L., 2013, "Mechanics of Adhered Pressurized Graphene Blister," ASME J. Appl. Mech. **80**(4), p. 040909.
[8] Cao, Z., Wang, P., Gao, W., Tao, L., Suk, J. W., Ruoff, R. S., Akinwande, D., Huang, R., and Liechti, K. M., 2014, "A Blister Test for Interfacial Adhesion of Large-Scale Transferred Graphene," Carbon, **69**, pp. 390–400.
[9] Liu, X., Boddeti, N. G., Szpunar, M. R., Wang, L., Rodriguez, M. A., Long, R., Xiao, J., Dunn, M. L., and Bunch, J. S., 2013, "Observation of Pull-In Instability in Graphene Membranes Under Interfacial Forces," Nano Lett., **13**(5), pp. 2309–2313.
[10] Boddeti, N. G., Liu, X., Long, R., Xiao, J., Bunch, J. S., and Dunn, M. L., 2013, "Graphene Blisters With Switchable Shapes Controlled by Pressure and Adhesion," Nano Lett., **13**(12), pp. 6216–6221.
[11] Stolyarova, E., Stolyarov, D., Bolotin, K., Ryu, S., Liu, L., Rim, K. T., Klima, M., Hybertsen, M., Pogorelsky, I., Pavlishin, I., Kusche, K., Hone, J., Kim, P., Stormer, H. L., Yakimenko, V., and Flynn, G., 2009, "Observation of Graphene Bubbles and Effective Mass Transport Under Graphene Films," Nano Lett., **9**(1), pp. 332–337.
[12] Georgiou, T., Britnell, L., Blake, P., Gorbachev, R. V., Gholinia, A., Geim, A. K., Casiraghi, C., and Novoselov, K. S., 2011, "Graphene Bubbles With Controllable Curvature," Appl. Phys. Lett., **99**(9), p. 093103.
[13] Bunch, J. S., Verbridge, S. S., Alden, J. S., van der Zande, A. M., Parpia, J. M., Craighead, H. G., and McEuen, P. L., 2008, "Impermeable Atomic Membranes From Graphene Sheets," Nano Lett., **8**(8), pp. 2458–2462.
[14] Herbig, C., Ahlgren, E. H., Schroder, U. A., Martinez-Galera, A. J., Arman, M. A., Kotakoski, J., Knudsen, J., Krasheninnikov, A. V., and Michely, T., 2015, "Xe Irradiation of Graphene on Ir(111): From Trapping to Blistering," Phys. Rev. B, **92**(8), p. 085429.
[15] Levy, N., Burke, S. A., Meaker, K. L., Panlasigui, M., Zettl, A., Guinea, F., Castro Neto, A. H., and Crommie, M. F., 2010, "Strain-Induced Pseudo-Magnetic Fields Greater Than 300 Tesla in Graphene Nanobubbles," Science, **329**(5991), pp. 544–547.
[16] Lu, J., Castro Neto, A. H., and Loh, K. P., 2012, "Transforming Moire Blisters Into Geometric Graphene Nano-Bubbles," Nat. Commun., **3**, p. 823.
[17] Pan, W., Xiao, J., Zhu, J., Yu, C., Zhang, G., Ni, Z., Watanabe, K., Taniguchi, T., Shi, Y., and Wang, X., 2012, "Biaxial Compressive Strain Engineering in Graphene/Boron Nitride Heterostructures," Sci. Rep., **2**, no. 893.
[18] Qi, Z., Kitt, A. L., Park, H. S., Pereira, V. M., Campbell, D. K., and Castro Neto, A. H., 2014, "Pseudomagnetic Fields in Graphene Nanobubbles of Constrained Geometry: A Molecular Dynamics Study," Phys. Rev. B, **90**(12), p. 125419.
[19] Zabel, J., Nair, R. R., Ott, A., Georgiou, T., Geim, A. K., Novoselov, K. S., and Casiraghi, C., 2012, "Raman Spectroscopy of Graphene and Bilayer Under Biaxial Strain: Bubbles and Balloons," Nano Lett., **12**(2), pp. 617–621.
[20] Yue, K., Gao, W., Huang, R., and Liechti, K. M., 2012, "Analytical Methods for the Mechanics of Graphene Bubbles," J. Appl. Phys., **112**(8), p. 083512.
[21] Wang, P., Gao, W., Cao, Z., Liechti, K. M., and Huang, R., 2013, "Numerical Analysis of Circular Graphene Bubbles," J. Appl. Mech., **80**(4), p. 040905.
[22] Arroyo, M., and Belytschko, T., 2004, "Finite Crystal Elasticity of Carbon Nanotubes Based on the Exponential Cauchy-Born Rule," Phys. Rev. B, **69**(11), p. 115415.

[23] Lu, Q., and Huang, R., 2009,"Nonlinear Mechanics of Single-Atomic-Layer Graphene Sheets," Int. J. Appl. Mech., **1**(03), pp. 443–467.
[24] Kudin, K. N., Scuseria, G. E., and Yakobson, B. I., 2001, "C2F, BN, and C Nanoshell Elasticity From Ab Initio Computations," Phys. Rev. B, **64**(23), p. 235406.
[25] Huang, Y., Wu, J., and Hwang, K. C., 2006, "Thickness of Graphene and Single-Wall Carbon Nanotubes," Phys. Rev. B, **74**(24), p. 245413.
[26] Lu, Q., Arroyo, M., and Huang, R., 2009, "Elastic Bending Modulus of Monolayer Graphene," J. Phys. D: Appl. Phys., **42**(10), p. 102002.
[27] Aitken, Z. H., and Huang, R., 2010, "Effects of Mismatch Strain and Substrate Surface Corrugation on Morphology of Supported Monolayer Graphene," J. Appl. Phys., **107**(12), p. 123531.
[28] Gao, W., Xiao, P., Henkelman, G., Liechti, K. M., and Huang, R., 2014, "Interfacial Adhesion Between Graphene and Silicon Dioxide by Density Functional Theory With van der Waals Corrections," J. Phys. D: Appl. Phys., **47**(25), p. 255301.
[29] Na, S. R., Suk, J. W., Ruoff, R. S., Huang, R., and Liechti, K. M., 2014, "Ultra Long-Range Interactions Between Large Area Graphene and Silicon," ACS Nano, **8**(11), pp. 11234–11242.
[30] Yoon, T., Shin, W. C., Kim, T. Y., Mun, J. H., Kim, T.-S., and Cho, B. J., 2012, "Direct Measurement of Adhesion Energy of Monolayer Graphene As-Grown on Copper and Its Application to Renewable Transfer Process," Nano Lett., **12**(3), pp. 1448–1452.
[31] Na, S. R., Suk, J. W., Tao, L., Akinwande, D., Ruoff, R. S., Huang, R., and Liechti, K. M., 2015, "Selective Mechanical Transfer of Graphene From Seed Copper Foil Using Rate Effects," ACS Nano **9**(2), pp. 1325–1335.
[32] Ishigami, M., Chen, J. H., Cullen, W. G., Fuhrer, M. S., and Williams, E. D., 2007, "Atomic Structure of Graphene on SiO_2," Nano Lett. **7**(6), pp. 1643–1648.
[33] Gupta, A., Chen, G., Joshi, P., Tadigadapa, S., and Eklund, P. C., 2006, "Raman Scattering From High-Frequency Phonons in Supported n-Graphene Layer Films," Nano Lett., **6**(12), pp. 2667–2673.
[34] Sonde, S., Giannazzo, F., Raineri, V., and Rimini, E., 2009, "Dielectric Thickness Dependence of Capacitive Behavior in Graphene Deposited on Silicon Dioxide," J. Vac. Sci. Technol. B, **27**(2), pp. 868–873.
[35] Springman, R. M., and Bassani, J. L., 2008, "Snap Transitions in Adhesion," J. Mech. Phys. Solids, **56**(6), pp. 2358–2380.
[36] Li, T., and Zhang, Z., 2010, "Snap-Through Instability of Graphene on Substrates," Nanoscale Res. Lett., **5**(1), pp. 169–173.
[37] Hencky, H., 1915, "On the Stress State in Circular Plates With Vanishing Bending Stiffness," Z. Math. Phys., **63**, pp. 311–317.